

Modelling of an updraft fixed-bed gasifier operated with softwood pellets

C. Mandl^{a,*}, I. Obernberger^{a,b}, F. Biedermann^b

^a Graz University of Technology, Institute for Process and Particle Engineering, Inffeldgasse 21b, A-8010 Graz, Austria

^b BIOS BIOENERGIESYSTEME GmbH, Inffeldgasse 21b, A-8010 Graz, Austria

ARTICLE INFO

Article history:

Received 30 September 2009

Received in revised form 12 July 2010

Accepted 13 July 2010

Available online 24 July 2010

Keywords:

Modelling

Gasification

Fixed bed

Wood pellets

ABSTRACT

This paper presents a one-dimensional steady state mathematical model for the simulation of a small scale fixed-bed gasifier. The model is based on a set of differential equations describing the entire gasification process of softwood pellets and is solved by a two step iterative method. The main features of the model are: homogeneous and heterogeneous combustion and gasification reactions, one-step global pyrolysis kinetics and drying, heat and mass transfer in the solid and gas phases as well as between phases, heat loss, particle movement and shrinkage within the bed. The pyrolysis model has been improved by partially cracking primary tar into lighter gases according to experimental data. The model is used to simulate a laboratory scale fixed-bed updraft gasifier. Good agreement is achieved between prediction and measurements for the axial temperature profiles and the composition of the producer gas. Moreover, results are presented for different air to fuel ratios and varying power inputs. The gasification process is improved by increasing the power input of the gasifier as a result of higher temperatures. Furthermore, a higher air to fuel ratio lowers the efficiency of the gasification process.

© 2010 Elsevier Ltd. All rights reserved.

1. Introduction

The gasification of renewable solid biomass to produce CO₂-neutral fuels for heat and electricity production is still in the development stage. Softwood pellets are presently used in small-scale residential combustion units. As the market is expected to further increase within the next years, pellets may also be used in small-scale fixed-bed gasifiers for heating purposes as well as regarding micro-CHP applications (e.g. Stirling engine or micro-turbine) in the near future. Due to the high tar content of the producer gas (up to 150 g/m³), updraft gasifiers are not suitable for engines and gas turbines without comprehensive gas cleaning. For the proper design of such gasifiers and for a better understanding of the gasification process appropriate models are needed. This paper presents a one-dimensional mathematical model as well as its validation and application.

Various models [1–7] dealing with the simulation of updraft fixed-bed gasifiers can be found in literature, but some of them are quite old or contain simplifying assumptions regarding physical properties and kinetics. Furthermore, the majority of the models have been applied to the gasification of coal. Focusing on the gasification of softwood pellets, only one model has been proposed so far [3]. An important fact is that mathematical models often contain complex differential equations resulting in extensive numerical solutions. One possibility to reduce the complexity of

the numerical solution is to use time-independent mathematical models, which is acceptable when focusing on steady-state operation. However, a description of the dynamic behaviour of the gasifier, which is primarily relevant for control purposes, is not possible.

The scope of this work was the modelling of the steady-state operation of a fixed-bed gasifier operated with softwood pellets with respect to proper reactor design and influence of changed operating conditions on the gasification process. Moreover, experiments have been carried out with a lab-scale gasifier and a comparison between model predictions and measurements is provided.

2. Mathematical model

Fig. 1 shows the basic geometry of the updraft gasifier presented in this paper.

The fuel (pellets) is fed continuously from the top of the gasifier, which can be considered as a simple cylindrical shaft, and forms a packed bed on the grate. The gasification air is injected from the bottom below the grate and passes through the fuel bed. Hot product gases exit the gasifier from the top, while the pellets descent toward the grate and are heated up successively by the gases. The fuel ash falls through the grate. The overall gasification process can be separated into four different reaction zones stratified along the reactor height – drying, pyrolysis, gasification and combustion. On the gasifier top the fuel is heated up by the hot gases and evaporation of fuel moisture usually starts immediately. Above

* Corresponding author. Tel.: +43 (0)316 873 4894; fax: +43 (0)316 873 104894.
E-mail address: mandl@bios-bioenergy.at (C. Mandl).

The energy equation for the solid phase is

$$-\sum_i \frac{\partial}{\partial z} (\rho_{i,\text{solid}} * cp_{i,\text{solid}} * T_{\text{solid}} * v_{\text{solid}}) = \frac{\partial}{\partial z} \left(\lambda_{\text{solid}} \frac{\partial T_{\text{solid}}}{\partial z} \right) - \sum r_{i,\text{solid}} * \Delta H_{r,\text{solid}} + W_{\text{sg}} + W_{\text{sw}} \quad (2)$$

The energy equation for the gas phase is

$$\sum_i \frac{\partial}{\partial z} (\rho_{i,\text{gas}} * cp_{i,\text{gas}} * T_{\text{gas}} * v_{\text{gas}}) = \frac{\partial}{\partial z} \left(\lambda_{\text{gas}} \frac{\partial T_{\text{gas}}}{\partial z} \right) - \sum r_{i,\text{gas}} * \Delta H_{r,\text{gas}} + W_{\text{sg}} + W_{\text{gw}} \quad (3)$$

The heat loss through the reactor walls is not neglected and is considered according to [4]

$$W_{\text{iw}} = \frac{4 * \alpha_{w,i}}{D_V} * (T_w - T_i) \text{ with } i = g, s \quad (4)$$

The heat transfer [21] between the solid and the gas phase is evaluated according to Eq. (5).

$$W_{\text{sg}} = \zeta * \frac{2.06 * cp_{\text{gas}} * \rho_{\text{gas}} * v_{\text{gas}}}{\varepsilon} * Re^{-0.575} * Pr^{-\frac{2}{3}} * A_p * (T_s - T_g) \quad (5)$$

The Reynolds number is calculated from the particle diameter, the velocity and the viscosity of the gas phase. A dimensionless correction factor ζ has been introduced before [1,6] to account for uncertainties regarding physical characteristics of the biomass and heat transfer effects in reacting systems. A performed sensitivity study has shown that ζ has only a moderate influence on the axial temperature profile of the packed bed. For this study a reference value of 0.5 has been chosen to produce realistic temperature values. The packed bed at any point is described by the specific surface area (A_p) and the void fraction ε . For simplicity, the void fraction is supposed to be constant, assuming that no fragmentation and agglomeration of the particles take place in the reactor. This assumption may only be valid for wood pellets because these pellets have a good mechanical strength and do not break up due to the pyrolysis, gasification and combustion process as it could be observed during experiments. Furthermore, possible wall effects on the void fraction of the bed are neglected as changes in the packing of the particles at the wall cannot be considered with a one-dimensional model. However, no aggregation of particles at the wall has been observed during experiments. The specific surface area (A_p) depends on the actual volume-equivalent diameter of the biomass particles and the void fraction of the bed and can be evaluated from Eq. (6) [11].

$$A_p = \frac{6 * (1 - \varepsilon)}{d_p} \text{ with } d_p = d_{p,0} * \sqrt{(1 - Y_{\text{ash}}) * \frac{v_{\text{solid}}}{v_{\text{solid},0}} + Y_{\text{ash}}} \text{ with } d_{p,0} = 3 \sqrt{1.5 * d_{\text{cylinder}}^2 * l_{\text{cylinder}}} \quad (6)$$

The volume-equivalent diameter of the initial particles is calculated from a cylinder with a diameter of 0.006 m and a length of 0.02 m, which are typical values for standardised softwood pellets. The diameter of the biomass particles and consequently the speed of the biomass are assumed to remain constant along the drying and pyrolysis zones, while the density of the biomass decreases. On the contrary, due to the heterogeneous reactions in the gasification and oxidation zone, the diameter of the biomass particles and consequently the speed of the biomass decrease according to the unreacted-core model with shrinking particle size [11], while the density of the biomass char remains constant. The changes of the

particle diameter induced by chemical reactions are taken into account with a shrinking particle diameter, depending on the ash content of the fuel and the actual velocity (v_{solid}) of the solid phase (Eq. (6)).

The conservation equations are considered for the solid and the gas phase species. For the solid phase the species biomass (wood pellets) and char are considered, the gas phase species are H_2O , CO , CO_2 , H_2 , CH_4 , tar, O_2 and N_2 . Furthermore, the fuel moisture is considered to be a part of the solid phase. For the species of the solid phase ρ is defined as a partial density.

$$\frac{\partial}{\partial z} (v_{\text{solid}} * \rho_{\text{wood}}) = -r_{p1} \quad (7)$$

$$\frac{\partial}{\partial z} (v_{\text{solid}} * \rho_{\text{char}}) = r_{p1} * v_{\text{char}} - M_{\text{char}} * (r_{c1} + \sum r_{g,i}) \quad (8)$$

$$\frac{\partial}{\partial z} (v_{\text{solid}} * \rho_{\text{moisture}}) = -m_{\text{water}} \quad (9)$$

The superficial velocity of the char in bulk can be evaluated from Eq. (10).

$$\frac{\partial v_{\text{solid}}}{\partial z} = -\frac{1}{\rho_{\text{char},0}} * M_{\text{char}} * (r_{c1} + \sum r_{g,i}) \quad (10)$$

The initial char density ($\rho_{\text{char},0}$) can be evaluated from Eq. (8). In the formulation of the conservation equation of the gas phase species turbulence and diffusion are not considered, thus the general form of the conservation equation of the gas phase species is

$$\frac{\partial \rho_{i,\text{gas}}}{\partial z} = \frac{1}{v_{\text{gas}}} * \left(r_{i,\text{gas}} - \rho_{i,\text{gas}} * \frac{\partial v_{\text{gas}}}{\partial z} \right) \quad (11)$$

The pressure drop in the gasifier is expected not to be negligible, primarily when a thick layer of ash is built up on the grate as it could be observed during experiments. Furthermore, a thick ash layer may have a significant influence on the gasification process as shown in Ref. [11]. On the other hand, the pressure drop of a packed bed of softwood pellets is supposed to be relatively small compared to the pressure drop caused by the ash layer. Thus, for all simulations carried out the ash layer is supposed to be small as the ash is periodically removed from the grate. Therefore, in the model approach the gasifier is assumed to be isobaric.

The speed of the gas phase can be evaluated from the continuity equation (Eq. (12)) of the gas phase.

$$\sum \frac{\partial}{\partial z} (\rho_{i,\text{gas}} * v_{\text{gas}}) = \sum r_{i,\text{gas}} + m_{\text{water}} \quad (12)$$

2.2. Kinetics

The overall gasification process can be separated into four different reaction zones stratified along the reactor height. For each zone the main physical properties and chemical reactions are considered for the model.

2.2.1. Drying

The drying process of the biomass is described by a 1st order kinetic equation depending on the temperature of the solid by means of an Arrhenius kind expression (Eq. (13)) [10]. Kinetic constants are derived from Ref. [10] and are listed in Table 2.

$$m_{\text{water}} = (\rho_{\text{moisture}}) * A_{\text{H}_2\text{O}} * \exp \left(-\frac{E_{\text{H}_2\text{O}}}{R * T_{\text{solid}}} \right) \quad (13)$$

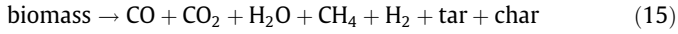
2.2.2. Pyrolysis

The devolatilization of biomass is a complex phenomenon, which involves a large number of chemical reactions. As usually

done in mathematical modelling of fixed-bed reactors, pyrolysis is described by a one-step global reaction (Eq. (14)).

$$r_{p1} = \rho_{\text{wood}} * A_{p1} * \exp\left(\frac{E_{p1}}{R * T_{\text{solid}}}\right) \quad (14)$$

The considered products of the global reaction are as following (Eq. (15)).



Tars often undergo secondary cracking reactions (r_{p2}) to form combustible gases CO and CH₄, CO₂ and water vapour [15].

$$r_{p2} = \rho_{\text{tar}} * A_{p2} * \exp\left(-\frac{E_{p2}}{R * T_{\text{gas}}}\right) \quad (16)$$

Condensation of tars is not considered, since the chemical composition and therefore the dew point of the tars are unknown. Furthermore, the temperatures in the upper fuel bed are expected to be relatively high due to the low moisture content of softwood pellets, so it can be assumed that most of the tars exit the gasifier in gaseous form. The composition of the products of the pyrolysis reactions r_{p1} and r_{p2} , taken from Refs. [1] and [15], are listed in Table 1.

The data regarding r_{p1} listed in Table 1 have been derived from experiments performed with beech wood particles. Sufficient experimental data for pyrolysis of softwood pellets could not be obtained. Kinetic constants for the primary reactions are taken from Ref. [17] and for the cracking reaction (Eq. (16)) of the tars from Ref. [35]. Tar is modelled as a lumped hydrocarbon with the proposed composition C₆H₈O [16] and a molecular weight of 96. The heat of reaction of the pyrolysis is assumed to be small compared to the heat of reaction related to combustion and gasification [13], so its effects are rather small. Therefore, the heat of reaction of the secondary pyrolysis reaction is not considered. For the primary pyrolysis a heat of reaction of 300 kJ/kg (endothermic) has been assumed to satisfy the overall energy balance of the pyrolysis.

The homogeneous water–gas (Eq. (17)) shift reaction is active in the pyrolysis and the drying zone as well and is modelled as a 1st order kinetic equation (Eq. (18)) [26].



$$r_{\text{wg}} = X_{\text{CO}} * X_{\text{H}_2\text{O}} * A_{\text{wg}} * \exp\left(-\frac{E_{\text{wg}}}{R * T_{\text{gas}}}\right) \quad (18)$$

Table 1
Product fractions (wt.%, d.b.) of the pyrolysis reactions [1,15].

	CO	CO ₂	H ₂ O	CH ₄	H ₂	tar	char
r_{p1}	4.5	10	11.5	0.3	0.2	48	25.5
r_{p2}	53.4	8.5	17	21.1	–	–	–

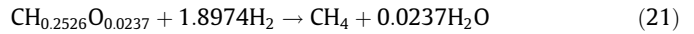
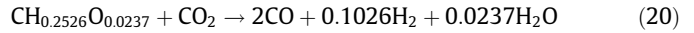
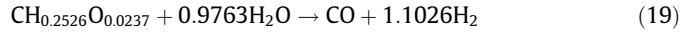
Table 2
Reference values for kinetic constants and heats of reaction.

Reaction	A	Unit	E (J kmol ⁻¹)	ΔH _R	Unit	Reference
m_{water} (13)	5.56×10^6	s ⁻¹	8.79×10^7	2250	kJ kg ⁻¹	[10]
r_{p1} (14)	$10^{4.03}$	s ⁻¹	77,800	350	kJ kg ⁻¹	[17]
r_{p2} (16)	2.076×10^3	s ⁻¹	66.3×10^6	0	–	[35]
r_{wg} (18)	1389	s ⁻¹	1.256×10^7	–41.2	kJ mol ⁻¹	[26]
$r_{g,\text{H}_2\text{O}}$ (19)	10^7	m s ⁻¹ K ⁻¹	1.256×10^8	172.6	kJ mol ⁻¹	[18,20]
r_{g,CO_2} (20)	10^7	m s ⁻¹ K ⁻¹	1.256×10^8	131.4	kJ mol ⁻¹	[18,20]
r_{g,H_2} (21)	10^4	m s ⁻¹ K ⁻¹	1.256×10^8	–75	kJ mol ⁻¹	[18,20]
r_{c1} (26)	4750	kg m ² s ⁻¹	2×10^8	–110.6/393.8	kJ mol ⁻¹	[22]
r_{c2} (31)	1.3×10^{11}	kmol m ³ s ⁻¹	1.256×10^8	–283	kJ mol ⁻¹	[11]
r_{c3} (34)	2.552×10^{14}	m ³ K ⁻¹ mol ⁻¹ s ⁻¹	9.304×10^7	–808.5	kJ mol ⁻¹	[27]
r_{c4} (35)	8.83×10^8	m ³ K ⁻¹ mol ⁻¹ s ⁻¹	9.976×10^7	–241.7	kJ mol ⁻¹	[27]

Kinetic constants of all reactions mentioned so far are listed in Table 2.

2.2.3. Gasification

In the gasification or reduction zone the model includes the heterogeneous reactions of the char. The char is modelled as hydrocarbon CH_{0.2526}O_{0.0237} [1] consisting primarily of carbon with small amounts of hydrogen and oxygen (elemental composition C = 95 wt.%, H = 2 wt.%, O = 3 wt.%). The following reactions are considered.



The reaction rate of a heterogeneous reaction depends on several effects (e.g. mass transfer in the gas phase, diffusion or chemical reaction). To account for these effects an overall reaction rate (Eq. (22)), depending on the mass transfer coefficient, the chemical reaction rate, the molar concentration of reacting gas phase species (H₂O, CO₂ and H₂) and the particle surface, is introduced.

$$r_{g,i} = \frac{X_i}{\frac{1}{k_g} + \frac{1}{r_{\text{chem},i}}} * A_p \quad \text{with } i = \text{H}_2\text{O}, \text{CO}_2, \text{H}_2 \quad (22)$$

$$r_{\text{chem},i} = A_i * \exp\left(-\frac{E_i}{R * T_{\text{solid}}}\right) \quad \text{with } i = \text{H}_2\text{O}, \text{CO}_2, \text{H}_2 \quad (23)$$

Kinetic constants (listed in Table 2) for the gasification reactions are taken from Ref. [18]. A literature correlation, taken from Ref. [21], is used for the mass transfer coefficient (Eq. (24)).

$$K_g = \frac{2.06 * V_{\text{gas}}}{\varepsilon} * Re^{-0.575} * Pr^{-\frac{2}{3}} \quad (24)$$

The values for the heat of reaction of the gasification reactions, listed in Table 2, are derived from Refs. [19] and [20].

2.2.4. Combustion

In the combustion zone the remaining biomass char is oxidized with the supplied air. Volatile products formed are burnt with oxygen to some extent. The combustion of char is a heterogeneous reaction. Similarly to the gasification reactions an overall reaction rate (Eq. (25)) is introduced. However, it has been proven that char combustion is predominantly controlled by diffusion rather than kinetics [11,23], so the chemical reaction rate ($r_{\text{chem},c1}$) of the char combustion is of minor relevance.

$$r_{cl} = \frac{PO_2}{\frac{1}{(2 * k_{\text{ox}})} + \frac{1}{\left(\frac{M_{\text{gas}}}{M_{\text{solid}}}\right) * r_{\text{chem},c1}}} * A_p \quad (25)$$

$$r_{\text{chem},c1} = A_{c1} * \exp\left(-\frac{E_{c1}}{R * T_{\text{solid}}}\right) \quad (26)$$

Kinetic constants for the combustion reaction (r_{c1}) are taken from Ref. [22]. A literature correlation, taken from Ref. [12], is used for the mass transfer coefficient (Eq. (27)).

$$k_{\text{ox}} = \frac{1.57 * v_{\text{gas}} * \rho_{\text{gas}} * Sc^{-\frac{2}{3}} * Re^{-0.41} * (1 - \varepsilon)^{0.2}}{M_{\text{gas}} * p} \quad (27)$$

The products of the char combustion are CO, CO₂ and water vapour (Eq. (28)), the stoichiometric coefficients can be calculated as

$$\begin{aligned} & \text{CH}_{0.2526}\text{O}_{0.0237} + \left(1 - 0.5\chi + \frac{0.2526}{4} - \frac{0.0237}{2}\right)\text{O}_2 \\ & \rightarrow \chi\text{CO} + (1 - \chi)\text{CO}_2 + \frac{0.2526}{2}\text{H}_2\text{O} \end{aligned} \quad (28)$$

The CO/CO₂ - ratio χ depends on the actual combustion temperature (Boudouard equilibrium) and can be evaluated from Eq. (29) [3].

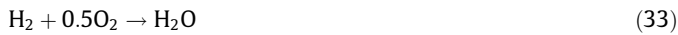
$$\chi = \left(\frac{k_{cc}}{1 + k_{cc}}\right) \text{ with } k_{cc} = 2500 * \exp\left(-\frac{6420}{T_{\text{solid}}}\right) \quad (29)$$

CO leaves the particle surface and is partly oxidized to CO₂ in the gas phase according to the following reaction (Eq. (30)). The reaction rate of the CO combustion (Eq. (31)) is derived from [11].



$$r_{c2} = \varepsilon * A_{c2} * X_{\text{CO}} * (X_{\text{O}_2})^{0.5} * (X_{\text{H}_2\text{O}})^{0.5} * \exp\left(-\frac{E_{c2}}{T_{\text{gas}}}\right) \quad (31)$$

Due to high combustion temperatures heterogeneous gasification reactions are already active in the combustion zone. Volatile products of these reactions leaving the particles are oxidized in the gas phase of the combustion zone to some extent. The following homogeneous gas phase reactions are considered (Eqs. (32) and (33))



The homogeneous gas phase reactions [27] are modelled as shown in Eqs. (34) and (35).

$$r_{c3} = \varepsilon * A_{c3} * X_{\text{CH}_4} * X_{\text{O}_2} * \exp\left(-\frac{E_{c3}}{T_{\text{gas}}}\right) \quad (34)$$

$$r_{c4} = \varepsilon * A_{c4} * X_{\text{H}_2} * X_{\text{O}_2} * \exp\left(-\frac{E_{c4}}{T_{\text{gas}}}\right) \quad (35)$$

Kinetic data for the methane combustion and for the hydrogen combustion are derived from Ref. [27]. All relevant kinetic data and heats of reaction for the combustion reactions are listed in Table 2.

2.3. Physical properties

Heat capacities of all species of the solid phase and for tar vapours are listed in Table 3. The specific heat capacity of tar is taken

Table 3
Reference values for heat capacities.

	cp (kJ kg ⁻¹ K ⁻¹)	Reference
Biomass (dry)	1.38	[17]
Char	$(420 + 2.09 * T_{\text{solid}} + 6.85 * 10^4 * T_{\text{solid}}^2) * 10^3$	[17]
Tar (vapour)	3.22	[12]
Water (liquid)	4.2	[12]

constant as the composition of tar is unknown and because there is no reliable approach, which accounts for changes in temperature.

The heat capacities of all gas phase species except for tar have been fitted from data taken from literature [28] by means of 4th order polynomials and are not listed in Table 3.

Thermal conductivity (Eq. (36)) and viscosity (Eq. (37)) of the gas are derived from [12].

$$\lambda_{\text{gas}} = \varepsilon * 4.8 * 10^{-4} * T_{\text{gas}}^{0.717} \quad (36)$$

$$\mu_{\text{gas}} = 1.98 * 10^{-5} * \left(\frac{T_{\text{gas}}}{300}\right)^{\frac{2}{3}} \quad (37)$$

The effective thermal conductivity (Eq. (38)) of the solid phase consists of the thermal conductivities of the individual species. In addition, due to expected high temperatures in the gasification and oxidation zone, radiation cannot be neglected and is taken into account by the thermal conductivity of the char. The effective thermal conductivity is modelled based on literature data derived from Refs. [10], [17] and [29].

$$\lambda_{\text{solid}} = k_{s0} * (\rho_{\text{wood}} + \rho_{\text{moisture}}) * \frac{1}{(\rho_{\text{wood}} + \rho_{\text{moisture}} + \rho_{\text{char}})} + \quad (38)$$

$$k_{\text{char}} * \rho_{\text{char}} / (\rho_{\text{wood}} + \rho_{\text{moisture}} + \rho_{\text{char}})$$

$$k_{s0} = 0.144 * \left((1.39 + 2.8 * 0.08 + 0.165) * \frac{\rho_{\text{solid},0}}{1000} \right) \quad (39)$$

$$k_{\text{char}} = 0.5 * k_{\text{rad},\text{gas}} + \frac{\varepsilon * 0.1046}{\left[\frac{0.1046}{(d_p * k_{\text{rad},\text{solid}})}\right] + 1.43 * (1 - 1.2 * \varepsilon)} \quad (40)$$

$$k_{\text{rad},\text{gas}} = 4 * \sigma * 0.05 * T_{\text{gas}}^3 \quad (41)$$

$$k_{\text{rad},\text{solid}} = 4 * \sigma * 0.85 * T_{\text{solid}}^3 \quad (42)$$

With k_{s0} the thermal conductivity of the wet biomass is considered. With k_{char} the thermal conductivity of the char is taken into account. Radiation is considered with the terms $k_{\text{rad},\text{gas}}$ and $k_{\text{rad},\text{solid}}$.

2.4. Numerical solution

One basic objective of the model processing was to find a simple but sufficiently accurate numerical solution for the model equations. Focusing on steady-state operation, the model is described by a set of highly non-linear, coupled, first order differential equations, that normally can be solved by an explicit finite difference method. Due to the countercurrent nature of the gas and solid flows resulting in a split-boundary value problem the model was solved by a developed code using a two step iterative method. In the first step guess values are used for the unknown boundary values on the top of the gasifier, as the simulation starts at the top of the gasifier (Fig. 1), and the model equations are solved by an ODE-solver (ode23) based on an explicit Runge–Kutta (2,3) method [30]. In the second step the unknown boundary values are varied using the secant method [31], until all boundary conditions at the top and at the bottom of the gasifier are satisfied. However, other iterative methods like the Newton's method converge faster, but the Newton's method requires the evaluation of both, function and its derivative at every step, while the secant method only requires the evaluation of the function itself. Since the evaluation of the derivatives of all governing equations is quite time-consuming and error-prone, the secant method was chosen for the iterative step.

At the top of the packed bed ($z = 0$) only solid phase properties are specified (Eq. (43)), as the composition and the temperature of the producer gas are unknown.

$$T_{\text{solid}} = T_0 \quad (43.1)$$

$$\rho_{\text{solid},0} = \rho_{\text{wood},0} + \rho_{\text{moisture},0} \quad (43.2)$$

$$\frac{\partial T_{\text{gas}}}{\partial z} = \frac{\partial T_{\text{solid}}}{\partial z} = 0 \quad (43.3)$$

At the bottom of the gasifier ($z = L$) the inlet air composition, temperature and mass flux of the gas phase are specified (Eq. (44)). The solid ash is assumed to be at ambient temperature, the solid mass flux can be related to the initial ash content of the biomass.

$$T_{\text{gas}} = T_{\text{solid}} = T_0 \quad (44.1)$$

$$\rho_i = 0 \text{ with } i = \text{CO}, \text{CO}_2, \text{H}_2, \text{CH}_4, \text{tar} \quad (44.2)$$

$$X_{\text{O}_2} = 0.21 \quad X_{\text{N}_2} = 0.785 \quad X_{\text{H}_2\text{O}} = 0.005 \quad (44.3)$$

3. Results

The model is used to simulate a laboratory scale fixed-bed up-draft gasifier.

3.1. Input parameter

Simulations have been carried out with the input parameters listed in Table 4 for steady-state operation. The bed to wall heat-transfer coefficients are chosen according to Ref. [1]. The gasifier (Fig. 2) consists of a cylindrical shaft, covered with an insulation made of ceramic fibres, and with an inner diameter of 0.125 m and a length of 0.6 m. The pellets are fed periodically to the gasifier in order to keep the bed at a constant height of approx. 0.45 m. A flat and circular grate with a crosswise agitator separates the ash disposal unit from the gasification unit. Ash is periodically discharged from the grate by activating the agitator to obtain continuous operation of the gasifier. The ash was usually burnt out well. The flow rate of the gasification air has been measured by means of a flow sensor in order to calculate the air to fuel ratio of the gasifier. The results of the simulation were compared with measurements derived from test runs performed with a laboratory-scale fixed-bed updraft gasifier. All experiments have been performed under stationary operating conditions of the gasifier. The temperature profile of the packed bed inside the gasifier has been measured

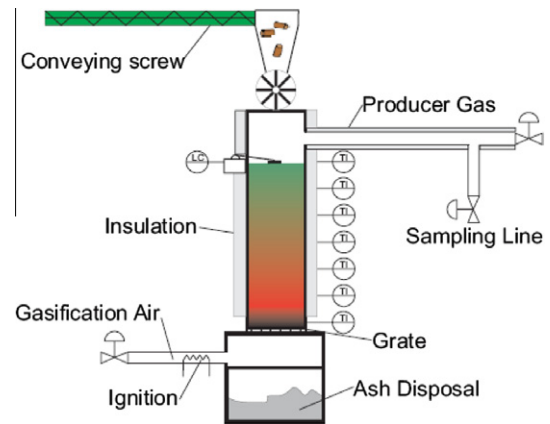


Fig. 2. Investigated small-scale updraft fixed-bed gasifier.

Table 5

Chemical characterisation of wood pellets. Explanations: moisture content in [wt.% w.b.]; ash content in [wt.% d.b.]; C-, H-, N-concentrations in [wt.% d.b.]; GCV ... gross calorific value [kJ/kg d.b.]; NCV ... net calorific value [kJ/kg w.b.].

	Pellets (softwood)
Moisture content	6.0
C	48.7
H	6.2
N	0.06
Ash content	0.4
GCV	19,676
NCV	17,060

by a set of thermocouples (Type K). To avoid channelling, the thermocouples have been stuck into the packed bed only periodically to measure the temperature in the middle of the bed at intervals of 5 cm.

Standardized softwood pellets (ÖNORM M 7135) were used for the test runs (see Table 5). The pellets have been analysed concerning the following parameters:

- moisture content: determination of weight loss at 105 °C
- ash content: method according to prCEN/TS 14775
- C, H, N: elemental analyser

Samples of the producer gas have been repeatedly taken at the outlet of the gasifier by means of gas collection tubes (Fig. 3).

Table 4
Input parameters for the simulation of the gasifier.

	Value
T_0	293 K
Solid mass	3.5 kg h ⁻¹
$\rho_{\text{solid},0}$	650 kg m ⁻³
$\rho_{\text{wood},0}$	598 kg m ⁻³
$\rho_{\text{char},0}$	152.5 kg m ⁻³
Y_{water}	8 wt.%
Y_{ash}	0.5 wt.% (db)
Air to fuel ratio	1.45 kg kg ⁻¹ (wb)
$\alpha_{w,\text{solid}}$	167 J m ⁻² s ⁻¹ K ⁻¹
$\alpha_{w,\text{gas}}$	1.256 J m ⁻² s ⁻¹ K ⁻¹
ζ	0.5
ε	0.5
$d_{p,0}$	0.0103 m
D	0.125 m
L	0.42 m

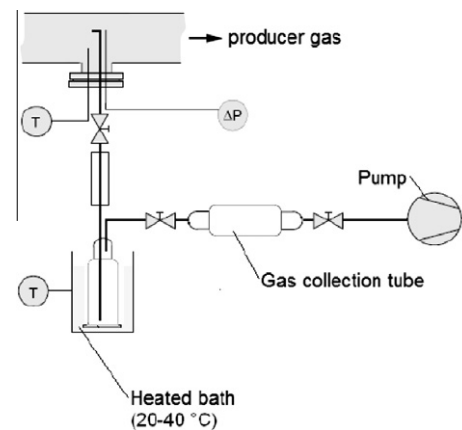


Fig. 3. Method for sampling of producer gas.

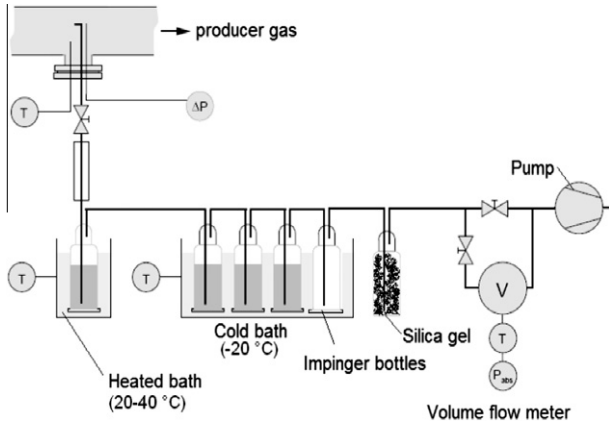


Fig. 4. Tar sampling train.

The samples have been cooled down to ambient temperature to remove tars. The composition of the producer gas was then measured by a micro Gas Chromatograph (CO, CO₂, H₂, CH₄, O₂ and N₂). The tar content of the producer gas was measured using a gravimetric method (Fig. 4) according to Ref. [34].

Samples of the producer gas are drawn through the impinger bottles that are filled with isopropanol as solvent. Heavy tars are collected in the bottles while light gases pass through. The overall volume flow of each sampling is measured by means of a volume flow meter. All samples are dried in a vacuum drier till all solvent is evaporated. The remaining tars are weighted and by means of the recorded volume flow during sampling the tar content of the producer gas is estimated in mg/Nm³ (d.b.). Tar is modelled as a lumped hydrocarbon with the proposed composition C₆H₈O and a molecular weight of 96. The molar concentration of the tar is calculated with this molecular weight. The composition of the tars (C, H and N) was measured using an elemental analyser. Due to the high tar content of the producer gas it was not possible to quantify the water content in the producer gas, but it was calculated from an oxygen mass balance with the input streams fuel mass and gasification air rate and the output streams of CO, CO₂, tar and H₂O.

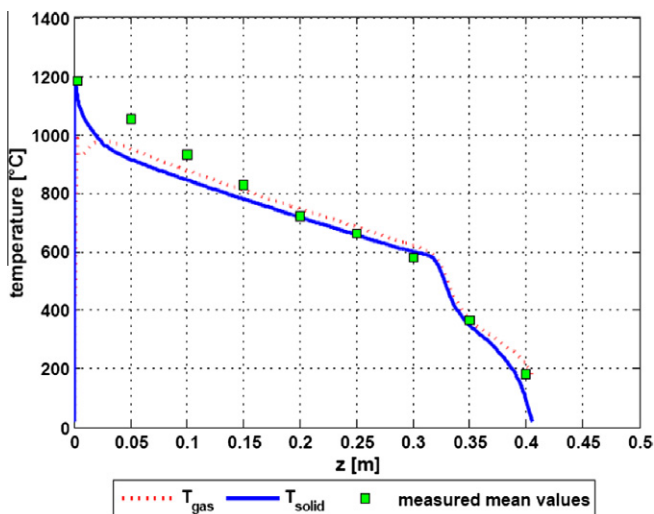


Fig. 5. Axial profiles of solid and gas phase temperatures – basic model. Explanations: dots refer to measured values; position of grate at z = 0 m; gasification agent: air; bed height constant at 0.42 m.

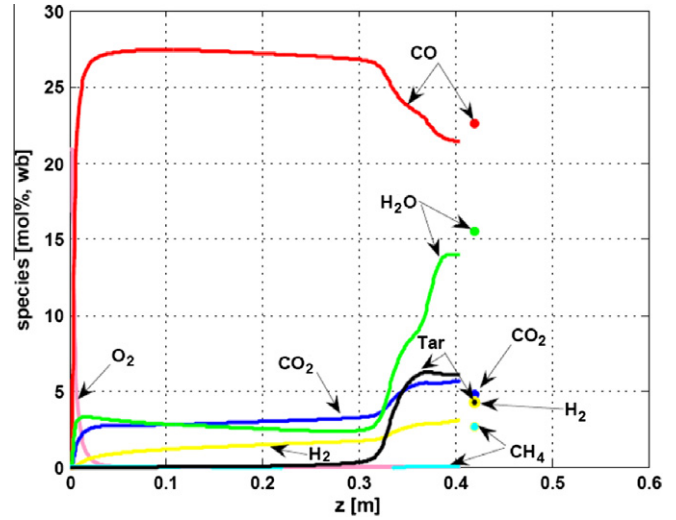


Fig. 6. Axial profiles of gas phase species – basic model. Explanations: dots refer to measured values; position of grate at z = 0 m; gasification agent: air; bed height constant at 0.42 m.

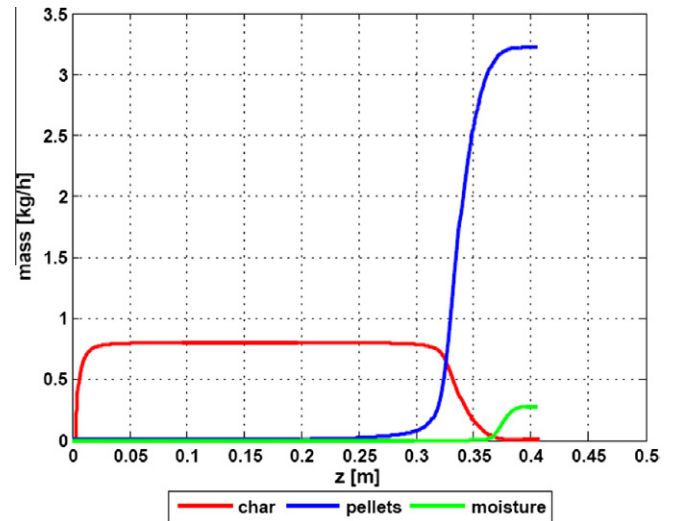


Fig. 7. Axial profiles of solid phase species – basic model. Explanations: position of grate at z = 0 m; gasification agent: air; bed height constant at 0.42 m.

3.2. Simulation results

In the Figs. 5–7 results of the simulations performed are shown. Fig. 5 shows the axial temperature profiles of the solid and the gas phase compared with the measurements taken from test runs. The axial profiles of the gas phase species (all shown concentrations are related to wet gas including tar) are illustrated in Fig. 6. Fig. 7 shows the axial profiles of the species of the solid phase. As fed to the gasifier the solid fuel is heated up by the product gas and evaporation of fuel moisture starts. The exit temperature of the producer gas is about 450 K, showing good agreement with the measurements. Due to the increased water content of the gas the water–gas shift reaction is active, which is indicated by the decreasing CO concentration.

At 500 K pyrolysis of the fuel starts indicated by distinctive gradients of temperature profiles and the decomposition of the fuel forming char and volatiles, respectively. Concentrations of the gas phase species increase rapidly in the pyrolysis zone apart from CO, which is the major product of the oxidation and gasification

zone. Furthermore, the water–gas shift reaction is active and CO₂ and H₂ increase. On the contrary, the CO concentration decreases. There is no satisfying agreement with the measurements regarding the producer gas composition as shown in Fig. 6. The calculated high tar content of the producer gas could not be observed during test runs. The tar content of the producer gas has been repeatedly measured according to a standardized method, described in Ref. [34], and results were repeatable. Furthermore, the energy balance of the gasifier was not consistent for higher tar contents. Therefore, it can be assumed that the tar measurements are reliable. The temperatures in the pyrolysis zone are too low in order to favour the cracking reactions of the tars [32]. The composition of the primary pyrolysis reaction has been taken from Ref. [1], whereas reported data has been derived from test runs carried out with beech wood particles [14]. The derived experimental data may not be suitable for softwood pellets and the operating conditions, respectively. This problem will be discussed in detail later.

As drying and pyrolysis of the wood pellets is completed, the residual char particles are heated by the up-streaming hot gases. It seems that there is a long zone, situated in the middle of the gasifier, where homogeneous reactions are slow and heterogeneous reactions do not occur (Fig. 7). However, the water gas shift reaction is active, but the dominant process is the heating of the char bed by the hot gases coming from the bottom of the gasifier. This has been reported by other authors [1,25,33] before and is in good agreement with measurements regarding the temperature profile.

Gasification and combustion are located along a thin zone at the bottom of the gasifier. As the air enters the gasifier, O₂ rapidly decreases as the char is burnt and the solid temperature attains high values. The steep gradients of the temperature profiles above the grate result from a very thin ash bed and because the air is supplied to the gasifier at ambient temperature. Consequently, the difference between solid and gas temperature is high above the grate and the dominant process is the heterogeneous combustion of char resulting in high CO values as the gas phase reactions (combustion of CO) are slower due to the lower gas temperature. Due to the char combustion the solid temperature attains values slightly below 1500 K. The calculated solid temperature above the grate shows good agreement with the measured temperature. The temperature profile has been measured with thermocouples that have been stuck into the packed bed. Therefore, they should represent the temperature of the solid phase. Furthermore, sintering of ash has been observed during experiments. Using standardized softwood pellets it can be stated that sintering of the ash usually occurs above approximately 1500 K.

As a result of the high temperature of the solid phase gasification of the char starts and the temperature of the solid phase decreases again due to the high endothermic nature of the gasification reactions. Again, CO is the major product of the gasification, The H₂ production is considerably smaller. The H₂ production could be increased by supplying humidified air or steam as gasification agent to the gasifier. There exists no strict spatial breakup between the combustion and gasification zone as competing reactions overlap each other. Heterogeneous gasification reactions start due to high temperature of the solid char although char combustion is still active. About 5 cm above the grate combustion reactions terminate indicated by the complete extinction of oxygen. Consequently, the solid and gas temperatures decrease due to the endothermic gasification reactions and all heterogeneous reactions expire.

3.3. Adaptation of pyrolysis

As already discussed no good agreement was achieved between prediction and measurement for the composition of the producer gas of the gasifier, probably caused by inadequate experimental

data for the pyrolysis zone. The product composition of the primary pyrolysis reaction strongly depends on the boundary conditions (e.g. heating rate, reactor temperature) of the experiment and of course the fuel itself. With means of characteristic pyrolysis temperatures and the existing gradients, an average residence time for the solid fuel in the pyrolysis zone can be estimated based on the measured temperature profile. The length of the pyrolysis zone is defined by two characteristic temperatures of the packed bed. At about 500 K pyrolysis of the fuel starts, which is indicated by an increasing temperature gradient in the packed bed (bed height approx. 0.35 m). As the pyrolysis of the fuel is complete, the temperature gradients in the packed bed decrease significantly (see Fig. 5). At a bed height of approx. 0.25 m temperature gradients reach very small values. The temperature of the packed bed at this point is the second characteristic pyrolysis temperature (850 K). The superficial velocity of the pellets in bulk along the drying and pyrolysis zone is assumed to be constant and is calculated from the initial bulk density of the fuel, the fuel feed rate and the diameter of the gasifier. Based on these assumptions, the residence time of the fuel is about 14 min resulting in a heating rate of 0.4 K/s. The composition of the primary pyrolysis reaction has been taken from [1], whereas reported data have been derived from test runs carried out with beech wood particles (mean particle diameter 5 mm) and a heating rate of about 1.6 K/s [14]. Based on the calculations it can be stated, that the operating conditions of the investigated gasifier differ from the conditions of the experiments in [14]. As it is well known, a higher heating rate favours the production of tars. The predicted tar content of the producer gas was considerably higher than the repeatedly measured value derived from test runs.

Therefore, the product composition of the primary pyrolysis reaction has been adapted as follows. As it is well-known, tars often undergo secondary cracking reactions forming lighter gases. Due to the moderate temperatures in the upper region of the packed bed of the gasifier, cracking of tars, as described by the model with the temperature depending reaction r_{p2} , does not occur. Therefore, the predicted tar content of the producer gas depends just on the product composition of the primary pyrolysis reaction. Since the boundary conditions of the experiment the pyrolysis data have been derived from differ from the conditions of the test runs performed with the laboratory-scale gasifier, the producer gas composition can only be influenced by changing the product composition of the primary pyrolysis reaction. Therefore, the tar ratio of the primary pyrolysis reaction has been reduced to fit to measured values and the remaining reported tar ratio undergoes a secondary reaction as described by Ref. [15]. The modified composition of the pyrolysis products is listed in Table 6.

Based on the new input data for the pyrolysis zone, simulations of the gasifier have been performed again. Remaining input parameters, listed in Table 3, have not been changed.

Fig. 8 shows the axial profiles of the gas phase species (all shown concentrations are related to wet gas including tar) based on the new parameters for pyrolysis. Due to the changed pyrolysis data, the predicted composition of the producer gas is now in rather good agreement with the measurements despite of an acceptable deviation related to CO₂ and H₂ (see Table 7).

Table 6

Reported and modified mass fractions (wt.% d.b.) of the primary pyrolysis reaction [1,15].

	CO	CO ₂	H ₂ O	CH ₄	H ₂	tar	char
r_{p1}	4.5	10	11.5	0.3	0.2	48	25.5
r_{p1}	11.7	11.1	13.8	3.2	0.2	34.5	25.5

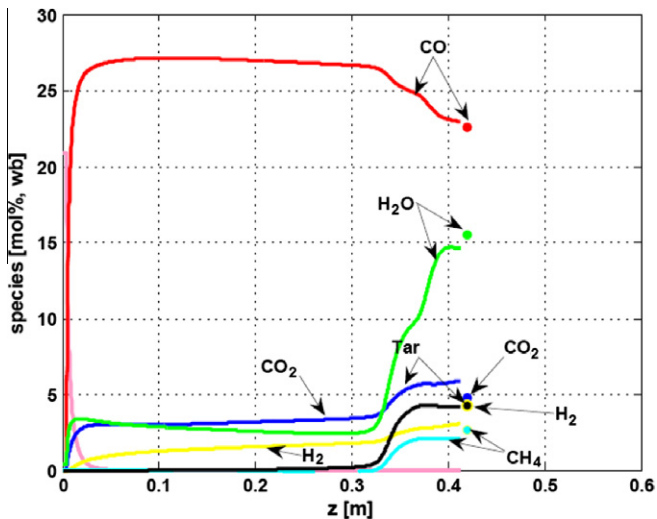


Fig. 8. Axial profiles of gas phase species – adapted model. Explanations: dots refer to measured values; position of grate at $z = 0$ m; gasification agent: air; bed height constant at 0.42 m.

Table 7

Results of simulations and test runs performed.

Producer gas		Measured	Calculated
CO	Vol% (wb)	22.6	22.9
CO ₂	Vol% (wb)	4.8	5.8
CH ₄	Vol% (wb)	2.7	2.1
H ₂	Vol% (wb)	4.3	3.1
tar	Vol% (wb)	4.3	4.2
H ₂ O	Vol% (wb)	15.5	14.6
NCV	MJ/Nm ³ (wb)	8.6	8.1
Gas outlet	°C	180	175

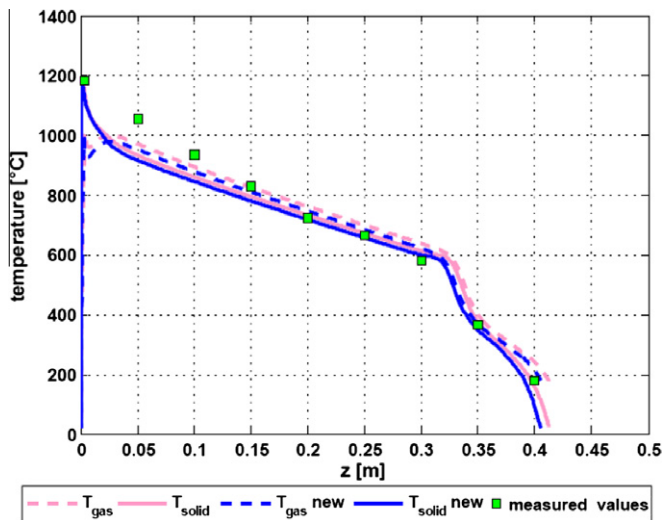


Fig. 9. Axial profiles of solid and gas phase temperatures – basic and adapted (new) model. Explanations: dots refer to measured values; position of grate at $z = 0$ m; gasification agent: air; bed height constant at 0.42 m.

The influence of the modified data on the temperature profiles of the solid and the gas phases is small as shown in Fig. 9. The outlet temperature of the producer gas decreases about 5 K due to the changed gas phase enthalpies in the pyrolysis zone.

Results of the simulations performed compared with experimental data derived from the test runs are listed in Table 7.

3.4. Changed operating conditions

For a better understanding of the gasification process and in order to show the influence of changed operating conditions on the operation of a fixed-bed gasifier, a parameter study has been carried out using the adapted model. The air to fuel ratio has been varied and the influence on the gasification process and the reliability of the results calculated by the model have been investigated.

Furthermore, the power input of the reactor has been varied by changing fuel (from 3 to 4 kg h⁻¹) and air rates. The air to fuel ratio was held constant for the simulations regarding the variation of the power input as well as the coefficients of the primary and secondary pyrolysis. The fuel rates have not been varied over a wider range, because the assigned air to fuel ratio is not longer valid as shown in Fig. 12.

Fig. 10 shows the temperature profiles of the solid and the gas phase for the variation of the power input. The molar fractions of CO and CO₂, the outlet temperatures and NCV of the producer gas against the fuel feed rate are shown in Fig. 11.

It can be seen that with higher fuel and air feed rates the temperatures along the packed bed increase also indicated by different producer gas outlet temperatures.

According to higher temperatures the CO yield increases corresponding to decreasing CO₂ values as shown in Fig. 10. The shown results of the simulations performed may conclude that the gasification efficiency increases with the power input. These results are basically in agreement with literature [1,24].

The concentrations of the other gas phase species (not shown here) are slightly influenced by the changed feed rates, which can be attributed to the constant coefficients of the primary and secondary pyrolysis. This assumption may not be correct as it is well known that the yields of char, volatiles and liquids of the pyrolysis depend on the heating conditions of the packed bed. Due to the simplified treatment of the pyrolysis by the model including fixed ratios of the products, the influence of the bed temperature on the product composition of the primary pyrolysis reaction cannot be simulated. The implementation of a more detailed pyrolysis mechanism as described in Ref. [36] may improve the prediction of the product ratios of pyrolysis.

Simulations have also been performed for different air to fuel ratios. Fig. 12 shows the results of several test runs performed with a lab-scale gasifier. During test runs the air to fuel ratio has been varied by changing the power input of the lab-scale gasifier significantly. The varying air to fuel ratio is a result of the performed test runs and can be explained as follows: a higher air flow rate and consequently higher gas velocities improve the combustion of the solid char due to an improved diffusion of the oxygen and temperatures along the packed bed increase. Higher temperatures favour the heterogeneous gasification reactions and more char is consumed in the gasification zone. On the contrary, a lower air flow rate decreases the combustion of the solid char due to lower gas velocities and lower reaction rates of the char combustion and temperatures along the packed bed decrease [9]. Due to the lower temperatures in the pyrolysis zone the amount of char produced from pyrolysis is higher as it is well known that the char ratio increases as the pyrolysis temperature decreases. Therefore, at lower fuel input (lower fuel and air amounts) more oxygen is needed to burn the char and the air to fuel ratio increases. The simulations have been performed according to the test runs in order to provide a reliable comparison between the results of test runs and the simulations. An overview about the operating conditions used for the simulations is listed in Table 8.

As already mentioned before, due to the changed air to fuel ratio resulting in changed temperature profiles of the packed bed in the pyrolysis zone, the char yield of the pyrolysis has been adapted

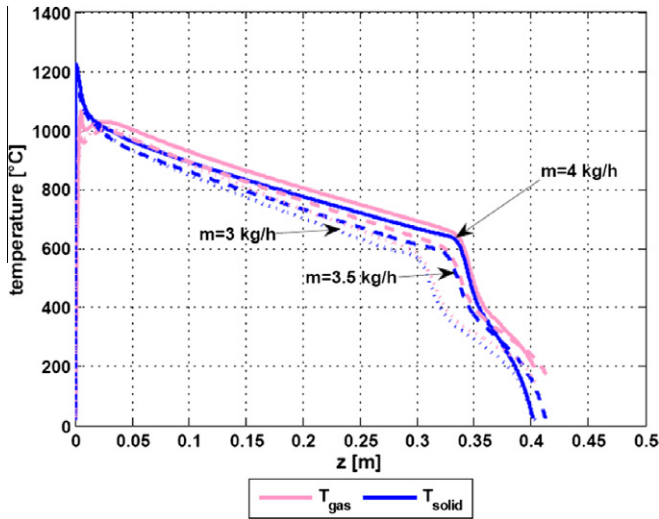


Fig. 10. Axial profiles of solid and gas phase temperatures – adapted model. Explanations: position of grate at $z = 0$ m; gasification agent: air; bed height constant at 0.42 m.

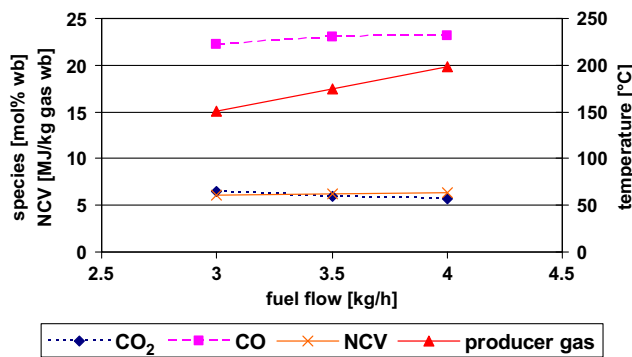


Fig. 11. Molar fractions of CO and CO₂ and producer gas outlet temperatures – adapted model. Explanations: position of grate at $z = 0$ m; gasification agent: air; bed height constant at 0.42 m.

(see Table 8) according to Ref. [1] to provide a complete burn out of the char in the combustion zone of the gasifier.

The temperature profiles of the solid and the gas phases for different air to fuel ratios as well as the corresponding measured values are shown in Fig. 13. Basically good agreement is obtained between the results of the simulations and the measurements. However, the calculated temperature profiles in the middle of the packed bed are too high for AF = 1.7. The over predicted values may conclude that the heat loss through the reactor wall is higher than estimated by the model.

Table 8
Input parameters for the simulation of the gasifier for different air to fuel ratios (AF).

			Unit
Air to fuel ratio	1.2	1.7	kg kg ⁻¹ (wb)
Equivalence ratio	0.2	0.28	–
Solid mass	3.5	1.25	kg h ⁻¹
$\rho_{solid,0}$	650	650	kg m ⁻³
Y_{water}	8	8	wt.%
Y_{ash}	0.5	0.5	wt.% (db)
T_0	293	293	K
H	0.42	0.42	m
Char ratio	20	28.5	wt.%

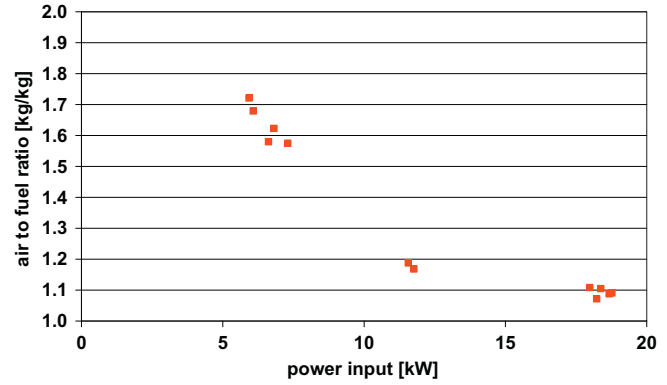


Fig. 12. Power input of gasifier against air to fuel ratio. Explanations: test runs performed with lab-scale gasifier under steady-state operation with softwood pellets; bed height constant at 0.42 m.

The calculated temperature of the producer gas at the outlet of the gasifier is higher for AF = 1.2 than the temperature measured during test runs. Because of the higher temperature of the producer gas calculated by the model the fresh biomass is heated up even faster. Moisture evaporation and pyrolysis of the pellets start immediately indicated by distinctive gradients of temperature profiles. Thus the calculated temperature profiles along the drying and pyrolysis zone differ from the measurements derived from the test runs.

The influence of different air to fuel ratios on the composition and the outlet temperature of the producer gas is illustrated in Fig. 14. An increase of the air to fuel ratio produces higher values of CO₂ and corresponding lower values of CO. In addition, a higher air flow rate (corresponding to a lower air to fuel ratio) and consequently higher gas velocities improve the combustion of the solid char due to an improved diffusion of the oxygen and temperatures along the packed bed increase as well as the producer gas outlet temperature.

The decreasing ratio of CO to CO₂ with increasing air to fuel ratios can be attributed to different temperatures in the combustion and gasification zone of the gasifier. Higher temperatures favour the production of CO from char combustion according to the Boudouard equilibrium and accelerate the reduction of CO₂ in the gasification zone. Furthermore, the concentration of nitrogen at the

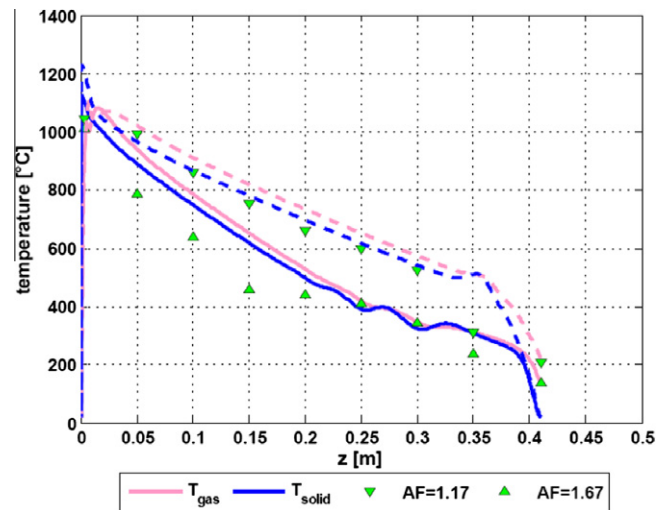


Fig. 13. Axial profiles of solid and gas phase temperatures for different air to fuel ratios – adapted model. Explanations: dots refer to measured values; position of grate at $z = 0$ m; gasification agent: air; bed height constant at 0.42 m.

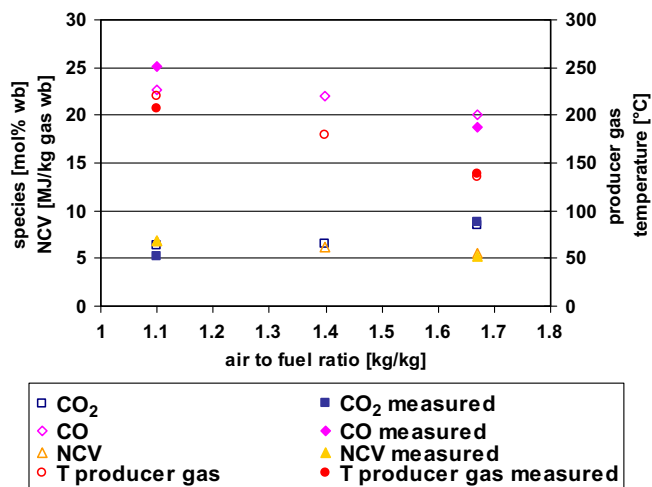


Fig. 14. Molar fractions of CO and CO₂, outlet temperatures and NCV of producer gas – adapted model. Explanations: position of grate at $z = 0$ m; gasification agent: air; bed height constant at 0.42 m.

Table 9

Results of simulations and test runs performed for AF = 1.2.

Producer gas		Measured	Calculated
CO	Vol% (wb)	25.1	22.7
CO ₂	Vol% (wb)	5.2	6.4
CH ₄	Vol% (wb)	1.6	3.2
H ₂	Vol% (wb)	4.9	3.1
tar	Vol% (wb)	4.6	4.7
H ₂ O	Vol% (wb)	18	16.8
NCV	MJ/Nm ³ (wb)	6.8	6.9
Gas outlet	°C	205	220

Table 10

Results of simulations and test runs performed for AF = 1.7.

Producer gas		Measured	Calculated
CO	Vol% (wb)	18.8	20.1
CO ₂	Vol% (wb)	8.8	8.4
CH ₄	Vol% (wb)	1.7	1.5
H ₂	Vol% (wb)	4.3	4.6
tar	Vol% (wb)	3.5	3.8
H ₂ O	Vol% (wb)	15.6	14.7
NCV	MJ/Nm ³ (wb)	5.2	5.6
Gas outlet	°C	140	135

outlet of the gasifier increases with higher air to fuel ratios which results in a dilution of the other components and a lower efficiency of the gasification process. Again, the results of the simulations are in quantitative agreement with the measurements derived from the test runs and with theoretical results reported in Ref. [1]. Results of the simulations performed compared with experimental data derived from the test runs are listed in Tables 9 and 10. The predicted composition of the producer gas is in rather good agreement with the measurements despite the deviations for AF = 1.2.

As already mentioned before, the deviation in the composition of the producer between measured and calculated values can be attributed to the simplified treatment of the pyrolysis by the model including fixed ratios of the products.

4. Conclusions

A one-dimensional steady state mathematical model for small-scale fixed-bed updraft gasifiers operated with softwood pellets

has been developed and solved. The model is based on a set of differential equations solved by a two step iterative method. Chemical and physical properties relevant for the gasification process have been derived from literature and implemented into the model. Simulations have been carried out for a laboratory-scale fixed-bed updraft gasifier and simulation results have been compared to measurements derived from test runs performed.

For the basic model good agreement is obtained between calculated and experimental results regarding the axial temperature profiles. The prediction of the composition of the producer gas was insufficient, probably caused by the simplified description of pyrolysis and insufficient data for the pyrolysis of softwood pellets. Primarily, the predicted high tar content could not be observed during test runs.

Therefore, the tar ratio of the primary pyrolysis reaction has been reduced to fit to measured values and the remaining reported tar ratio undergoes a secondary reaction forming lighter gases as described by Ref. [15]. Using the adapted model simulations have been performed again. Due to the changed pyrolysis data the predicted composition of the producer gas is in good agreement with the measurements despite of a deviation related to CO₂ and H₂. For the axial temperature profiles good agreement is obtained as well.

Furthermore, simulations for different air to fuel ratios and varying power inputs have been performed using the adapted model. With higher power input temperature profiles increase due the improved char combustion as well as the CO yield increase corresponding to decreasing CO₂ values. This may conclude that the gasification efficiency increases with the power input.

The concentrations of the other gas phase species are slightly influenced by the changed feed rates, which can be attributed to the constant coefficients of the primary pyrolysis. Due to the simplified treatment of the pyrolysis by the model including fixed ratios of the products, the influence of changed bed temperature on the product composition of the primary pyrolysis reaction cannot be simulated. For different air to fuel ratios simulation results show moderate agreement with measurements regarding the axial temperature profiles. Probably, the heat loss through the reactor wall was not proper calculated. The composition of the producer gas is in fair agreement with the measurements for the investigated air to fuel ratios. In fact, a higher air to fuel ratio lowers the efficiency of the gasification process.

The simulation model enables a good quantitative prediction of the small-scale updraft fixed-bed gasifier. The gasifier model can be a useful tool for the prediction of the temperature profiles and relevant output variables like producer gas composition and the air to fuel ratio as well as particularly for a proper reactor design.

The treatment of the pyrolysis zone may be the weakest part of the model, but more experimental data are required in order to achieve improvements. Furthermore, the implementation of a more detailed pyrolysis mechanism may improve the prediction of the product ratios of pyrolysis, which will be a major part of future work.

The model is also suitable for other biomass fuels like wood chips, but adjustment of physical properties and pyrolysis data is necessary.

Acknowledgement

The financial support of the Austrian Research Promotion Agency (FFG) is gratefully acknowledged.

References

- [1] Di Blasi C. Modeling wood gasification in a countercurrent fixed-bed reactor. *AIChE J* 2004;50(9).

- [2] Kayal TK, Chakravarty M, Biswas GK. Mathematical modelling of steady state updraft gasification of jute stick particles of definite sizes packed randomly – an analytical approach. *Bioresour Technol* 1997;60:131–41.
- [3] Lucas C. High temperature air/steam gasification of biomass in an updraft fixed bed batch type gasifier. PhD thesis. KTH, 2005.
- [4] Usman Ghani M, Radulovic Predrag T, Douglas Smoot L. An improved model for fixed-bed coal combustion gasification: sensitivity analysis applications. *Fuel* 1996;75(10):1213–26.
- [5] Brundo M. A mathematical model for coal and biomass gasification in a fixed bed reactor. In: 3rd international conference on clean coal technologies for our future, 2007.
- [6] Hobbs ML, Radulovic PT, Smoot LD. Combustion and gasification of coals in fixed beds. *Progr Energy Combust Sci* 1993;19:505–86.
- [7] Hobbs ML, Radulovic PT, Smoot LD. Modelling fixed-bed coal gasifiers. *AIChE J* 1992;38:681–702.
- [8] Gould LA. Chemical process control: theory and applications. Addison Wesley; 1969.
- [9] Bellais M. Modelling of the pyrolysis of large wood particles. PhD thesis. Stockholm: KTH; 2007.
- [10] Purnomo DJ. Model for a downdraft solid fuel combustor. PhD thesis. The University of Wisconsin; 1998.
- [11] Cooper J, Hallett WLH. A numerical model for packed-bed combustion of char particles. *Chem Eng Sci* 2000;55:4451–60.
- [12] Rosa L, Tosato R. Modelling and testing a cogeneration plant based on wood gasification. In: 7th European conference on industrial furnaces and boilers, 2006.
- [13] Rath J et al. *Fuel* 2003;82:81–91.
- [14] Di Blasi C, Signorelli G, Portoricco G. Countercurrent fixed-bed gasification of biomass at laboratory scale. *Ind Eng Chem Res* 1999;38:2571–81.
- [15] Rath J, Staudinger G. Cracking reactions of tar from pyrolysis of spruce wood. *Fuel* 2001;80:1379–89.
- [16] Thunman H, Niklasson F, Johnsson F, Leckner B. Composition of volatile gases and thermochemical properties of wood for modeling of fixed or fluidized beds. *Energy Fuel* 2001;15:1488–97.
- [17] Grønli M. A theoretical and experimental study of the thermal degradation of biomass. PhD thesis. Trondheim: NTNU; 1996.
- [18] Groeneveld MJ, van Swaaij WPM. Gasification of char particles with CO₂ and H₂O. *Chem Eng Sci* 1980;35:307–13.
- [19] Wang Y, Kinoshita CM. Kinetic model of biomass gasification. *Sol Energy* 1993;51:19–25.
- [20] Babu BV, Sheth Pratik N. Modeling and simulation of reduction zone of downdraft biomass gasifier: effect of char reactivity factor. *Energy Convers Manage* 2005.
- [21] Usman Ghani M et al. Fbed-1: fixed bed coal combustion and gasification model with a generalized coal devolatilization submodel (FG-DVC), measurement and modeling of advanced coal conversion processes, vol. III, 1993.
- [22] Bhagat PM. Wood charcoal combustion the effects of water application. *Combust Flame* 1980;37:275–91.
- [23] Bauer R et al. Modelling of grate combustion in a medium scale biomass furnace for control purposes. *Biomass Bioenergy* 2010;34:417–27.
- [24] Bryden KM, Ragland KW. Numerical modeling of a deep fixed bed combustor. *Energy Fuel* 1996;10:269–75.
- [25] Raupenstrauch H. Ein Beitrag zur Computersimulation reagierender Schüttschichten. PhD thesis. Technische Universität Graz; 1991.
- [26] Biba V, Macak J, Klose E, Malecha J. Mathematical model for the gasification of coal under pressure. *Ind Eng Chem Process Des Dev* 1978;17:92–8.
- [27] Deng Z et al. Computational fluid dynamics modeling of coal gasification in a pressurized spout-fluid bed. *Energy Fuel* 2008;22:1560–9.
- [28] VDI-Wärmeatlas. Verein deutscher Ingenieure. Springer Verlag; 1997.
- [29] Goldman J et al. A comparison of prediction and experiment in the gasification of anthracite in air and oxygen-enriched/steam mixtures. In: 20th symposium (international) on combustion. p. 1365–72.
- [30] Bogacki P, Shampine LF. A 3(2) pair of Runge–Kutta formulas. *Appl Math Lett* 1989;2:1–9.
- [31] Bartsch H-J. Taschenbuch mathematischer Formeln, 19. Auflage. Fachbuchverlag Leipzig im Carl Hanser Verlag; 2001.
- [32] Morf PO. Secondary reactions of tar during thermochemical biomass conversion. PhD thesis. ETH Zürich; 2001.
- [33] Raupenstrauch H. Gasdurchströmte chemisch reagierende Schüttschichten, Habilitationsschrift. Technische Universität Graz; 1997.
- [34] CEN technical specification. Biomass gasification-tar and particle in product gases-sampling and analysis. Prepared by CEN task force TC BT/TF 143 WICSC 03002.2, 2005.
- [35] Uden Ag, Berruti F, Scott DS. A kinetic model for the production of liquids from the flash pyrolysis of biomass. *Chem Eng Commun* 1988;65:207–21.
- [36] Di Blasi C. Modeling chemical physical processes of wood biomass pyrolysis. *Progr Energy Combust Sci* 2006;34:47–90.